Structure of an Engineered Porcine Phospholipase A2 with Enhanced Activity at 2.1 Å Resolution. Comparison with the Wild-type Porcine and Crotalus atrox Phospholipase A2

Thunnissen, Marjolein M.G.M.; Kalk, Kor H.; Drenth, Jan; Dijkstra, Bauke W.

Published in:
Default journal

Publication date:
1990

J. Mol. Biol. (1990) **216**, 425–439

Structure of an Engineered Porcine Phospholipase A_2 with Enhanced Activity at 2·1 Å Resolution

Comparison with the Wild-type Porcine and *Crotalus atrox* Phospholipase A_2

Marjolein M. G. M. Thunnissen, Kor H. Kalk, Jan Drenth and Bauke W. Dijkstra

Laboratory of Chemical Physics, University of Groningen
Nijenborg 16, 9747 AG Groningen, The Netherlands

(Received 6 April 1990; accepted 12 July 1990)

The crystal structure of an engineered phospholipase A_2 with enhanced activity has been refined to an *R*-factor of 18·6% at 2·1 Å resolution using a combination of molecular dynamics refinement by the GROMOS package and least-squares refinement by TNT. This mutant phospholipase was obtained previously by deleting residues 62 to 66 in porcine pancreatic phospholipase A_2, and changing Asp59 to Ser, Ser60 to Gly and Asn67 to Tyr. The refined structure allowed a detailed comparison with wild-type porcine and *Crotalus atrox* phospholipase A_2. The conformation of the deletion region appears to be intermediate between that in those two enzymes. The residues in the active center are virtually the same. An internal hydrophobic area occupied by Phe63 in the wild-type porcine phospholipase A_2 is kept as conserved as possible by local rearrangement of neighboring atoms. In the mutant structure, this hydrophobic pocket is now occupied by the disulfide bond between residues 61 and 91. A detailed description of the second binding site for a calcium ion in this enzyme is given.

1. Introduction

Phospholipase A_2 (PLA_2†, phosphatide acylhydrolase, E.C. 3.1.1.4) catalyzes the hydrolysis of the 2-acylesterbond of 3-*sn*-glycerophospholipids in a calcium-dependent reaction (Waite, 1987). The enzyme can be found both inside and outside the cell. Extracellular phospholipases A_2 occur abundantly in mammalian pancreatic tissue and juice and in snake and bee venoms. The enzymes from mammalian pancreas and snake venom show a high degree of sequential homology (Waite, 1987; Volwerk & de Haas, 1982), and the intracellular phospholipases A_2 appear to be homologous (Mizushima *et al.*, 1989; Seilhamer *et al.*, 1989; Kramer *et al.*, 1989). The pancreatic PLA_2 is produced in the pancreas as a zymogen. Upon secretion into the duodenum the proenzyme is activated by trypsin, which cleaves off seven N-terminal amino acid residues. For the snake venom PLA_2s, the existence of a zymogen is not known (Nieuwenhuizen *et al.*, 1974).

One of the intriguing properties of phospholipases A_2 is the fact that they show quite different behavior towards monomeric and aggregated substrates. While the mammalian proenzyme and the mature enzyme have a similar activity on monomeric substrates, the mature enzyme hydrolyzes aggregated substrates with much higher rates than it does monomeric substrates. The proenzyme does not show this activation by aggregated substrates (Pieterson *et al.*, 1974). The much higher rates of hydrolysis of aggregated substrates imply that the enzyme must recognize lipid/water interfaces, and that it probably possesses a binding site for aggregated substrates. Indeed, several residues have been identified by chemical modification to be part of this recognition site and were shown to affect the enzyme's properties with respect to the binding of aggregated substrates. On the basis of these studies, it was concluded that Leu2, Trp3, Arg6, Leu19 and Tyr69 are part of the binding site for aggregated substrates (Volwerk & de Haas, 1982). The three-dimensional structure of the bovine pancreatic PLA_2 showed that these residues are on one face of the protein molecule, around the entrance of the active site cleft (Dijkstra *et al.*, 1981). From these observations it was concluded that the binding site for aggregated substrates is an extended area

† Abbreviations used: PLA_2, phospholipase A_2; Δ62-66 PLA_2 mutant, porcine PLA_2 with residues 62 to 66 deleted and additional mutations D59S, S60G and N67Y; r.m.s., root-mean-square; bis-Tris, bis(2-hydroxyethyl)amino-tris(hydroxymethyl)methane.

0022–2836/90/220425–15 $03.00/0

around the active site cleft. Residues 65, 67, 70 and 72 were proposed to be part of this binding site (Dijkstra *et al.*, 1981). These latter residues have not been further analyzed by chemical modification methods.

In the pancreatic phospholipases A_2, residues 65 to 70 occur in a surface loop. A comparison of the structures of the mature bovine phospholipase A_2 and the bovine proenzyme shows that in the proenzyme this surface loop (comprising residues 62 to 72) and a part of the N-terminal helix are flexible or disordered, but that they have a well-defined conformation in the mature enzyme (Dijkstra *et al.*, 1982). The same flexibility was observed in the structure of the N-terminally transaminated bovine phospholipase A_2, which has the same kinetic properties as the proenzyme (Dijkstra *et al.*, 1984). An explanation for this difference in mobility in mature and proenzyme can be found in the fact that the 62–72 loop is linked *via* a hydrogen-bonding system to the N-terminal α-NH_3^+ group. When this hydrogen-bonding system is disrupted, as is the case in both the proenzyme and the N-terminally transaminated enzyme where no free α-NH_3^+ exists anymore, the 62–72 loop and part of the N-terminal helix become flexible. Because the proenzyme and the transaminated enzyme do not show any increase in activity when the substrate concentration is above the critical micelle concentration, it was concluded that these enzymes do not have an intact binding site for aggregated substrates and that the 62–72 loop is important for the regulation of the enzyme's activity towards aggregated substrates (Dijkstra *et al.*, 1984).

Interestingly, sequences of snake venom phospholipases A_2 show a deletion of five to eight residues in this loop (see Table 1). It is one of the most conspicuous sequence differences (Waite, 1987). Also, the kinetic properties and substrate specificity of snake venom phospholipases A_2 are rather different. The snake venom phospholipases A_2 have in general higher turnover numbers and have a higher affinity for phospholipid molecules aggregated in micelles than do the pancreatic phospholipases A_2. The pancreatic PLA_2s are in general more active towards negatively charged phospholipids (van Eyk *et al.*, 1983; Verhey *et al.*, 1981).

In an attempt to investigate the influence of these residues on the catalytic activity, residues 62 to 66 in the porcine PLA_2 were deleted (Kuipers *et al.*, 1989*a*). To increase the sequential homology with elapid snake venom PLA_2, a few other mutations were performed: Asp59Ser, Ser60Gly and Asn67Tyr (see Table 1). The glycine at position 60 was introduced because it was thought that the enzyme needed at that position a residue with a larger conformational freedom in order to form the proper disulfide bridge between cysteine 61 and cysteine 91. The Tyr at position 67 was introduced because in many snake venom phospholipases A_2 an aromatic residue is found at this position. Ser at position 59 is found in many of the elapid snake venom PLA_2s (Dennis, 1983). The construction and characterization of this mutant phospholipase A_2 (Δ62-66 mutant) and a preliminary description of its structure were given by Kuipers *et al.* (1989*a*). The Δ62-66 mutant showed a 16-fold increase in activity on micellar (zwitterionic) short chain lecithins compared to the native porcine PLA_2. The hydrolysis of phospholipid monomers is twice as fast. The structure at 2·5 Å (1 Å = 0·1 nm) resolution revealed that the biggest difference between the wild-type porcine and the Δ62-66 mutant porcine PLA_2 structure is found in the deleted loop area and in the topology of the binding site for aggregated substrates.

Here, we report the structure of the Δ62-66 mutant, refined at 2·1 Å resolution to a final *R*-factor of 18·6%. Both molecular dynamics refinement and conventional least-squares refinement procedures have been applied. A detailed description of the structure and a comparison with the structure of wild-type phospholipase A_2 is given.

2. Materials and Methods

(a) *Crystallization and data collection*

The Δ62-66 PLA_2 mutant was generously provided to us by the group of H. M. Verhey, A. J. Slotboom and G. H. de Haas (State University, Utrecht).

The freeze-dried protein was dissolved in 0·1 M-sodium acetate (pH 4·5) to a final concentration of 10 mg/ml. This solution was dialyzed overnight against 100 mM-bis-Tris·HCl (pH 7·0) with 5 mM-$CaCl_2$ added, in order to prevent rapid precipitation. The enzyme was crystallized at room temperature by vapor diffusion in hanging drops. The reservoir solution contained 1 ml of a solution of 50% (v/v) methanol in 100 mM-bis-Tris·HCl (pH 7·0), 5 mM-$CaCl_2$. Drops of 6 μl were formed by equal mixing of 3 μl of protein solution and 3 μl of the reservoir

Table 1

Comparison of part of the sequences of the mutant PLA_2 and of 3 native PLA_2s

	50					55						60						65					70				
(a)	H	D	N	C	Y	R	D	A	K	N	L	D	S	C	K	F	L	V	D	N	P	Y	T	E	S	Y
(b)	*	*	*	*	*	G	E	*	E	K	I	S	G	*	—	—	..	..	—	—	W	*	*	I	K	T	*
(c)	*	*	C	*	*	G	K	*	T	—	—	*	—	*	..	..	..	..	..	—	*	*	K	*	V	*	*
(d)	*	*	*	*	*	*	*	*	*	*	*	S	G	*	—	--	—	—	—	—	Y	*	*	*	*	*	*

(a) Porcine pancreatic PLA_2; (b) *Naja melanoleuca* PLA_2 fraction DE-III; (c) *C. atrox* PLA_2; and (d) mutant Δ62-66 PLA_2. The sequence numbering is according to Renetseder *et al.* (1984). An asterisk (*) denotes homology with the porcine sequence. Absent amino acid residues are indicated by a dash.

Table 2
Completeness of data

Resolution (Å)	Before†		After†	
	Completeness (%)	R_{merge}‡	Completeness (%)	R_{merge}‡
∞–10·00	58·8	2·36	58·8	2·36
10·00– 7·07	85·3	3·15	85·3	3·16
7·07– 5·77	92·5	3·56	92·5	3·56
5·77– 5·00	91·0	3·91	91·0	3·93
5·00– 4·47	91·8	4·43	91·8	4·44
4·47– 4·08	91·3	4·69	91·3	4·70
4·08– 3·78	92·0	4·70	92·0	4·70
3·78– 3·54	92·2	5·06	92·0	5·07
3·54– 3·33	93·4	5·48	93·1	5·48
3·33– 3·16	94·4	5·83	93·8	5·90
3·16– 3·02	93·6	5·82	88·6	5·82
3·02– 2·89	92·7	6·04	86·5	6·11
2·89– 2·77	92·8	7·24	82·1	7·15
2·77– 2·67	92·3	7·94	82·7	7·61
2·67– 2·58	89·0	8·90	74·3	8·59
2·58– 2·50	89·6	8·75	77·5	8·45
2·50– 2·43	87·7	9·20	73·4	8·18
2·43– 2·36	87·1	12·01	72·8	11·04
2·36– 2·29	83·7	11·35	68·1	10·57
2·29– 2·24	82·1	11·29	67·6	10·95
2·24– 2·18	77·8	12·09	65·0	11·52
2·18– 2·13	74·8	12·80	61·1	11·96
2·13– 2·09	71·8	15·43	61·1	14·46
Total	87·0	5·54	78·4	5·29

† Before and after removal of strongly deviating reflections with $l \leq -11$ (see the text for explanation).

‡ $R_{merge} = \dfrac{\sum_{hkl}\sum_{refl.} |I(hkl,j) - \bar{I}(hkl)|}{\sum_{hkl}\sum_{refl.} I(hkl)}$.

solution. Crystals suitable for X-ray analysis grew within 1 week. The crystals are platelets about 0·7 mm × 0·3 mm × 0·15 mm in size. The spacegroup is $P2_1$. There are 2 molecules of 119 residues each in an asymmetric unit.

Data up to 2·1 Å resolution were collected from 1 crystal with cell dimensions $a = 45{\cdot}8$ Å, $b = 73{\cdot}4$ Å, $c = 37{\cdot}3$ Å and $\beta = 107{\cdot}4°$ on an Enraf-Nonius FAST area detector, equipped with a CAD4 kappa-goniostat, with graphite monochromatized CuKα radiation from an Elliot GX-21 rotating anode generator. Data collection and reduction were carried out using the program system MADNES (Pflugrath & Messerschmidt, 1986). The crystal was mounted in a glass capillary with its *b*-axis approximately parallel to the capillary axis. The capillary with the crystal was positioned such that it was more or less aligned with the goniostat's ϕ-axis. The ϕ-axis was set so as to make an angle of about 36° with the ω-axis of the goniostat (thus the crystal's *b*-axis and the ω-axis do not coincide). This was done to optimize collection of a virtually complete dataset. Data were collected by rotation about the ω-axis using 2 different ϕ-settings of the crystal 90° apart, one at $\phi = 145°$ and one at $\phi = 234°$. At the 1st setting, 180° of oscillation were collected. However, due to radiation damage, only 130° could be collected at the 2nd setting. The resulting dataset contained 30,069 usable observations, 13,801 of which were unique reflections. The data had $R_{merge} = 0{\cdot}055$ for 12,278 *hkl* values (for a definition of R_{merge} see the legend to Table 2).

The overall completeness was 89·7%. Data were divided into chunks with $\Delta\phi = 10°$, scaled (Hamilton *et al.*, 1965) and merged together into a single dataset using programs of the Groningen BIOMOL protein structure determination software package. Deviating reflections (reflections not within 2·24 σ from the mean intensity) were omitted. The completeness of the dataset decreased to 87·0% after this procedure. Because the refinement did not converge (see below), we reassessed the quality of our data at a later stage. After a local scaling procedure it appeared that reflections with $l \leq -11$ had relatively very high *R*-factors (up to 80%). These reflections were omitted. The completeness decreased thereby to 78·4%. In order to find an explanation for these high *R*-factors, the whole data collection procedure was checked. It was observed that most of these reflections were collected in the later stages of the data collection. Most probably we underestimated the effect of (anisotropic) radiation decay. Table 2 gives an overview of the completeness and R_{merge} as a function of resolution both before and after the removal of these deviating reflections.

(b) *Refinement*

It has been shown that energy refinement combined with molecular dynamics simulation can be very powerful at the initial stages of a refinement procedure (Gros *et al.*, 1989*a*). Molecular dynamics techniques allow a molecular system to explore a larger conformational space than is possible with the more conventional methods of least-squares refinement (Brünger, 1988; Fujinaga *et al.*, 1989; Gros *et al.*, 1989*b*). We started molecular dynamics refinement with the GROMOS MDXREF program (Fujinaga *et*

al., 1989). As a starting model we used the partially refined structure at 2·5 Å resolution of the Δ62-66 mutant without water molecules (Kuipers *et al.*, 1989*a*). A 1st *R*-factor with data between 6 and 2·1 Å was 33% ($R = \Sigma||F_o|-|F_c||/\Sigma|F_o|$). The water molecules were omitted in order to avoid problems in the initial molecular dynamics runs carried out at higher temperatures (Gros *et al.*, 1989*b*).

The 1st refinement cycle was started by energy minimization with X-ray constraints followed by molecular dynamics simulation with X-ray constraints at 600 K, at relatively low resolution (8·0 to 3·5 Å). After this step, the temperature was slowly decreased to 300 K and in the mean time the resolution was gradually expanded from 3·5 to 2·9 Å. This refinement cycle lasted 3·3 ps. At the end of this 1st cycle, the *R*-factor was 27·8% (8 to 2·9 Å resolution). The model was inspected in a SIGMAA weighted $2F_o-F_c$ map (Read, 1986), in the later stages also OMIT maps were used (Bhat & Cohen, 1984; Bhat, 1988). All model building was done on an Evans & Sutherland PS390 system using the program FRODO (Jones, 1978). For the analysis of the results, the programs WHATIF (Vriend, 1990) and BIOGRAF (BIOGRAF, Biodesign Corporation, Pasadena, U.S.A.) were also used. Only minor rebuilding was done. At this stage 31 water molecules were added to the model.

After this manual intervention, a 2nd cycle of molecular dynamics refinement was performed. The whole cycle was done at a temperature of 300 K during 2·7 ps. While the resolution was gradually expanded to 2·7 Å, the *R*-factor decreased to 25·6% (8 to 2·7 Å resolution) at the end of this cycle. Because the refinement did not converge anymore at this stage, neither with the MDXREF program nor with the TNT package, we reprocessed our data to remove data that suffered too much from radiation damage (see above).

At this stage we switched to the least-squares refinement procedure of TNT (Tronrud *et al.*, 1987) instead of the molecular dynamics refinement, because of less severe central processing unit requirements. Cycles of alternating TNT refinement and model building were performed. A summary is given in Table 3. Water molecules were located in F_o-F_c maps. Peaks with a density $\geq 2\ \sigma$ were identified and used as possible water positions by the program PEKPIK from the XTAL package (Hall & Stewart, 1987). Only water molecules at proper distances from protein atoms were kept. Errors in the structure were found by careful inspection of Ramachandran plots (Ramakrishnan & Ramachandran, 1965) and the geometrical analysis part of TNT. Water molecules that developed *B*-factors higher than 55 Å^2 were removed from the model.

The refined co-ordinates for this PLA_2 Δ62-66 mutant have been deposited with the Protein Databank, Chemistry Department, Brookhaven National Laboratory, Upton NY 11973, U.S.A. (reference number 3P2P).

3. Results

(a) *Refinement*

After completion of the refinement, the crystallographic *R*-factor had decreased to 18·6% for all data between 6 and 2·1 Å resolution. The final model contains 204 water molecules and three calcium ions: one in the active site of each PLA_2 molecule and one on a non-crystallographic 2-fold axis between the two molecules in the asymmetric unit (monomer 1, residues 1 to 124; monomer 2, residues 201 to 324). The density for both molecules is clear (Fig. 1), except for residues around the β-wing tip, residues 79 and 80, in both molecules, where the density is weak. Also, some of the residues at the surface of the molecule have their side-chains in weak density. The C-terminal end of monomer 2 is disordered and no density is visible for residues

Table 3

Refinement statistics

A. *Progress of refinement*

Cycle	Number of rounds	Resolution (Å)	Start *R* (%)	End *R* (%)	Water molecules and rebuilding
1st MD	3·3 ps	8·0–3·5 s 8·0–2·9 e	33·5	27·8	Added 31 water molecules, minor rebuilding
2nd MD	2·7 ps	8·0–2·9 s 8·0–2·7 e	27·8	25·6	Added 65 water molecules, minor rebuilding
1 TNT	175 *xyz* 25 *B*	8·0–2·8 s 8·0–2·1 e	25·6	22·6	Added 70, removed 20 water molecules, rebuilding
2 TNT	135 *xyz* 35 *B*	8·0–2·1	25·6	20·2	Added 80, removed 16 water molecules, minor rebuilding
3 TNT	70 *xyz* 10 *B*	6·0–2·1	23·6	19·6	Removed 6 water molecules, rebuilding
4 TNT	120 *xyz* 28 *B*	6·0–2·1	22·1	18·6	

B. *Geometry statistics after completion of the refinement*

r.m.s. bond length deviations (Å)	0·010
r.m.s. bond angle deviations (°)	2·591
r.m.s. trigonal non-planarity deviations (Å)	0·006
r.m.s. planarity deviations (Å)	0·010
r.m.s. non-bonded interaction deviations (Å)	0·044

MD, molecular dynamics; s, at start of refinement cycle; e, at end of refinement cycle.

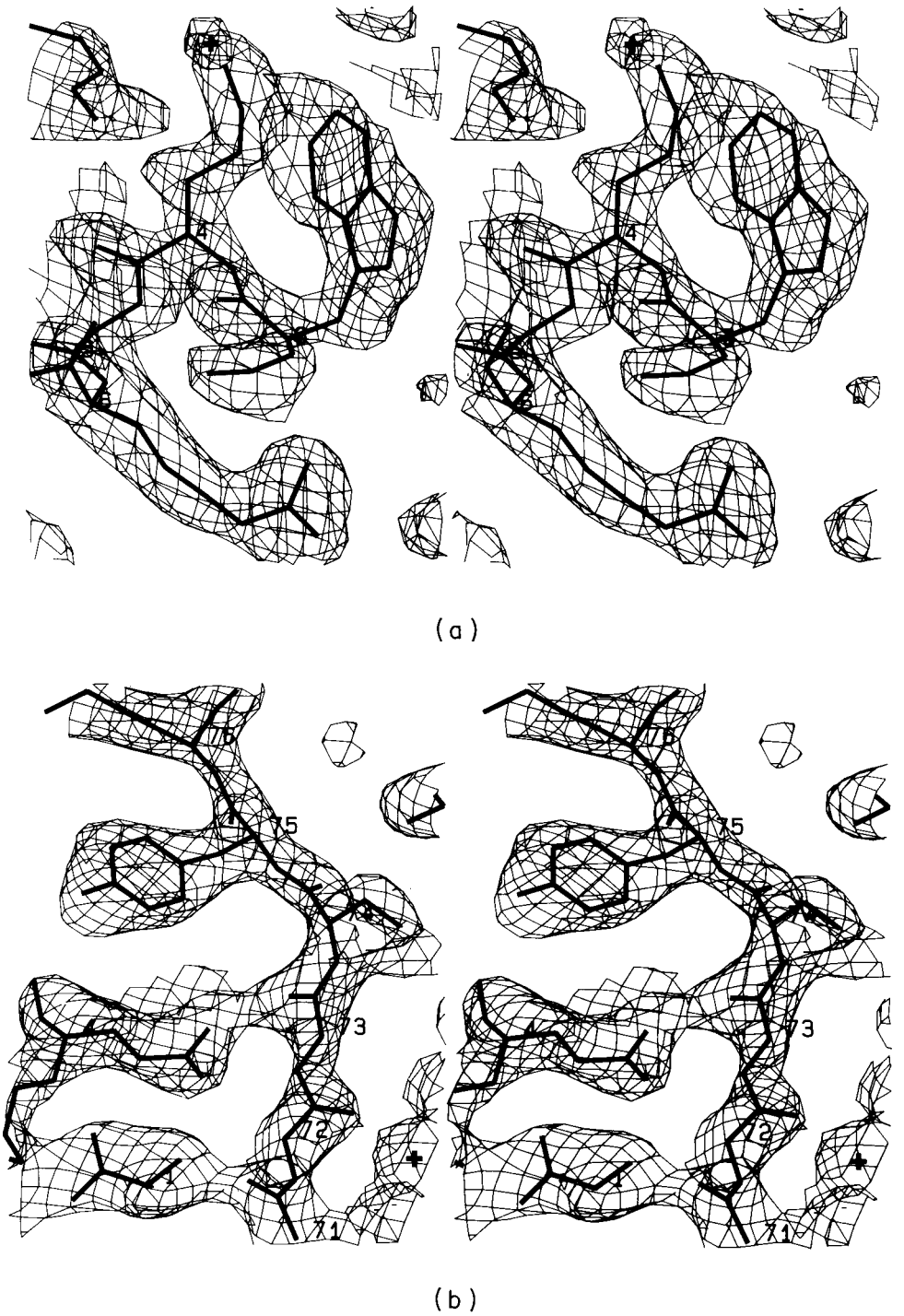

Figure 1. Stereo pictures showing $(2mF_o - DF_c)$, α_c (Read, 1986) electron density for parts of the map. The density is contoured at 1·1σ. (a) Trp3 to Arg6 at the N-terminal region of monomer 1. (b) Ser72 to Ser76 (main chain) of monomer 1.

319 to 323. Residue Cys324, which is connected to Cys227 by a disulfide bond, is visible again. In both monomers the density for the deletion region is clear and could easily be interpreted using OMIT maps and $2F_o - F_c$ maps (Fig. 2). From a Luzzati plot, the r.m.s. positional error in the co-ordinates is estimated to be 0·25 Å (Luzzati, 1952). An independent estimate of the error can be deduced from the r.m.s. difference in positions of the C^α atoms after superposition of the two monomers. The r.m.s. difference between all 119 C^α positions is 0·52 Å. If the most deviating atoms are omitted, this difference decreases to 0·35 Å for 101 C^α pairs. Details about the refinement and the quality of the structure can be found in Table 3.

The final Ramachandran plot is shown in Figure 3. The only three residues that are strongly deviating from the allowed regions are Thr80 and

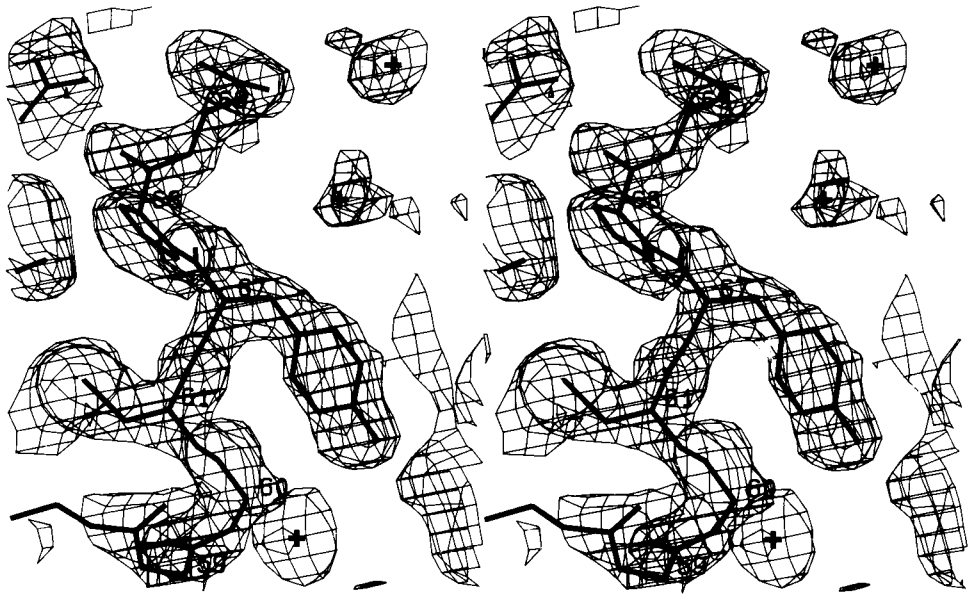

Figure 2. Stereo picture showing the $(2mF_o - DF_c)$, α_c (Read, 1986) electron density for the deletion region (residues 59 to 69) in monomer 1. The density is contoured at $1{\cdot}1\sigma$.

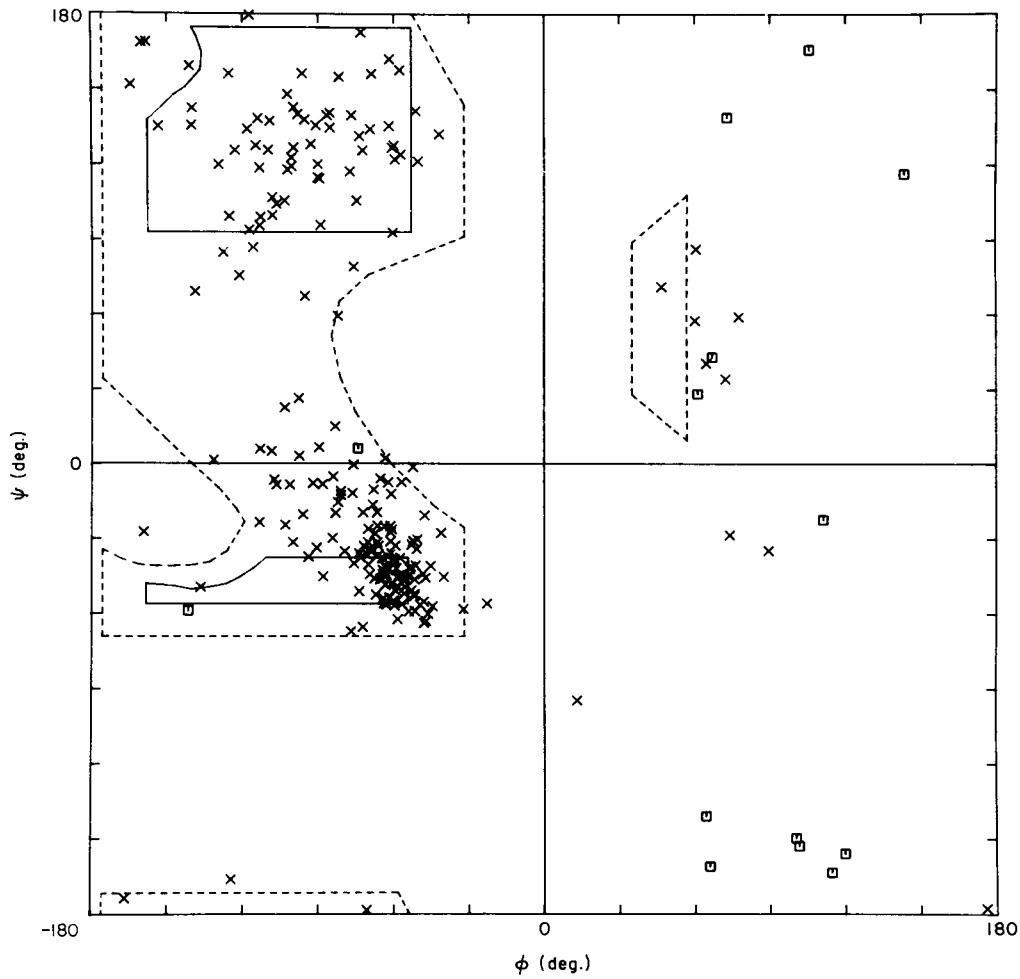

Figure 3. The ϕ, ψ plot of both monomers of the Δ62-66 mutant. The ϕ, ψ angles of non-glycine residues are indicated by a cross and those of glycine residues by a square. The continuous lines define the area of fully allowed conformations with $\tau(N, C^\alpha, C) = 110°$ for the non-glycine residues. The broken lines show the regions obtained by relaxing the van der Waals' contact constraints as well as by allowing the bond angle τ at C^α to increase to 115° (Ramakrishnan & Ramachandran, 1965). Strongly deviating residues are Thr80 ($\phi = 62°$, $\psi = -29°$), Thr280 ($\phi = 91°$, $\psi = -32°$) and Lys317 ($\phi = 14°$, $\psi = -89°$).

Thr280, both located in the β-wing tip, and Lys317 located in the disordered C terminus of monomer 2.

(b) *Comparison of the two molecules in the asymmetric unit*

In the asymmetric unit, two protein molecules are present that are related to each other by a non-crystallographic axis ($\kappa = 178{\cdot}3°$). This 2-fold axis constitutes the most conspicuous contact between the two monomers and it runs through a calcium ion that is ligated by atoms from both monomers (see below). In the wild-type porcine PLA_2 structure, this calcium-binding site is also present, but there it is found on a crystallographic 2-fold axis. The overall structure of the two monomers in the asymmetric unit is almost the same, including the conformation of the deletion region, but three stretches with differences occur. All these differences are caused by different intermolecular contacts (see Fig. 4 and Table 4).

The first of these stretches can be found around Pro14. A hydrogen bond exists between the carbonyl oxygen of Pro214 and the $N^{\eta 1}$ atom of Arg43, but this hydrogen bond is not present between the carbonyl oxygen of Pro14 and the $N^{\eta 1}$ of Arg243, because these atoms are more than 10 Å apart. As a result the C=O of Pro14 is in a different position and, as a consequence, Gly15 has quite different ϕ, ψ angles in both monomers (Gly15 $\phi = 111{\cdot}5°$, $\psi = -22{\cdot}5°$; Gly215 $\phi = -96{\cdot}5°$, $\psi = 156{\cdot}3°$).

The second stretch is around Leu31 and involves the first calcium-binding site. In both monomers the calcium site is formed by the same residues, and the configuration around the calcium ion is hardly changed, but the conformation of Leu31 in both monomers is completely different. In monomer 2, Leu231 has hydrophobic interactions with a symmetry-related molecule, but in monomer 1 this residue is totally exposed to the solvent (see Table 4).

The last deviating stretch is found at the C terminus. In monomer 1, the COO^- group of the C terminus makes a salt bridge with Arg206 from a crystallographically related molecule. In addition, this Arg206 is hydrogen-bonded to the carbonyl oxygen of Lys122. Hydrophobic interactions occur between Tyr123 and Leu319, and the side-chain of Lys121 is hydrogen-bonded to the carbonyl oxygen of Ser86 of a symmetry-related molecule. In monomer 2, none of these interactions occurs, and this most probably explains why in monomer 2 residues 319 to 323 are disordered or flexible.

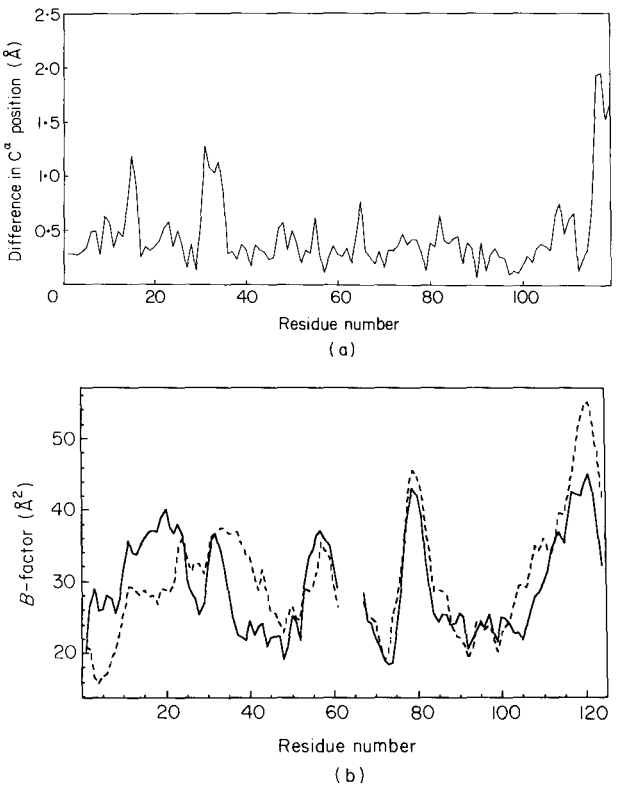

Figure 4. (a) Differences in C^α positions (in Å) after superimposing monomer 1 and monomer 2. (b) Temperature factors (Å^2) of the C^α atoms as a function of residue number for the 2 monomers: heavy line, monomer 1; broken line: monomer 2.

Table 4

Differences in intermolecular contacts between the 2 monomers in the asymmetric unit

Monomer 1		Monomer 2	
Site 1; around Pro14			
C^α Pro14–C^β Leu231	3·8 Å	O Pro214–$N^{\eta 1}$ Arg43	2·6 Å
C^β Pro14–C^β, $C^{\delta 1}$ & C Leu231	3·8–4·0 Å		
C Pro14–C^β Leu231	3·8 Å		
Site 2; around Leu31			
No intermolecular interactions		C^β Leu231–C^α, C^β Pro14	3·8–4 Å
		$C^{\delta 1}$ Leu231–C^β Pro14	3·9 Å
		C Leu231–C^β Pro14	4·0 Å
Site 3; around the C terminus			
N^ζ Lys121–O Ser86	3·0 Å	N^ζ Lys322–O Cys77	3·7 Å
O Lys122–$N^{\eta 2}$ Arg206	2·9 Å		
C^β Tyr123–$C^{\delta 1}$ Leu319	3·5 Å		
$C^{\delta 1}$ Tyr123–C^γ Leu319	3·7 Å		
O Cys124–$N^{\eta 1}$ Arg206	2·7 Å		

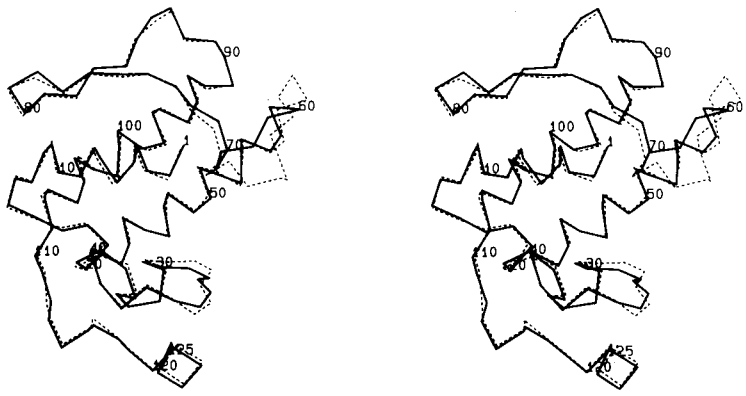

Figure 5. Comparison of a C^{α} backbone tracing of wild-type (dotted lines) and Δ62-66 mutant PLA_2 (heavy lines).

(c) *Comparison with wild-type porcine phospholipase A_2*

In Figure 5, a comparison is shown between the Δ62-66 mutant and the wild-type porcine PLA_2, the structure of which has been refined at 2·6 Å resolution to an *R*-factor of 24·1% (Dijkstra *et al.*, 1983). The greater part of these structures is virtually the same. As expected, the largest differences are found in the deletion area, residues 59 to 70.

In wild-type porcine PLA_2, these residues form a short surface loop from residue 59 to 66 and then one and a half turns of 3_{10} helix from residues 66 to 70. Specific interactions of this loop with the rest of the molecule are made by Cys61, which forms a disulfide bridge with Cys91, and by Phe63, which is in the interior of the protein and fills up a hydrophobic pocket. This pocket is formed by the side-chains of Pro68, Ala55, Leu58, Ile95, the disulfide bridge between Cys61 and Cys91, and the backbone atoms of Glu71. The 61–91 disulfide bridge is at the surface of the protein and shields this hydrophobic pocket from the solvent. All the interactions of these residues are given in Table 5.

In the Δ62-66 mutant, the loop 59 to 70 becomes shortened and the 3_{10} helix part is not present anymore. Residues 59 and 60 form a turn, residues 61 to 68 have an extended conformation, and residues 69 and 70 are positioned in another turn (Fig. 6).

The most conspicuous changes occur around residue 63. In the Δ62-66 mutant, Phe63 is deleted, but the hydrophobic pocket occupied by this residue still exists. Instead of Phe63, the disulfide bridge between Cys61 and Cys91 moves to the interior of the protein and fills this pocket. The C^{α} of Cys61 thereby changes 4·4 Å in position, and the side-chain of Cys91 has to rotate 180° around the C^{α}–C^{β} bond to make a proper disulfide bridge (Fig. 7). The rest of Cys91 does not change. The pocket itself has hardly changed in conformation. The biggest change here is effected by Pro68 moving

Table 5

Interactions of residues 59 to 70 in porcine and Δ62-66 mutant PLA_2

Residues	Porcine PLA_2	Residues	Δ62-66 PLA_2 mutant
Asp59	Surface residue, no specific interactions	Ser59	Surface residue, no specific interactions
Ser60	Surface residue, no specific interactions	Gly60	Surface residue, no specific interactions
Cys61	Surface residue, disulfide bridge to 91, hydrophobic interactions with Phe63	Cys61	Surface residue, disulfide bridge to 91, hydrophobic interactions with several residues, C=O interaction with a water molecule
Lys62	Surface residue, $N^{\delta 2}$ interaction to C=O Phe63	—	—
Phe63	Interior residue, phenyl ring, several hydrophobic interactions, C=O interaction with $N^{\delta 2}$ Lys62 and N Val65	—	—
Leu64	Surface residue, hydrophobic interactions with Thr70, C=O interaction with N Asn67	—	—
Val65	Surface residue, interaction with Asn67, N interaction with C=O of Phe63	—	—
Asp66	Surface residue, C=O interaction with N^{ζ} Lys56	—	—
Asn67	Surface residue, $O^{\delta 1}$ interaction with $O^{\gamma 1}$ Thr70, N interaction with C=O Leu64	Tyr67	Surface residue, no specific interactions
Pro68	Interior residue, hydrophobic interactions with Phe63	Pro68	Interior residue, hydrophobic interactions with disulfide bridge 61–91
Tyr69	Surface residue, no specific interactions	Tyr69	Surface residue, no specific interactions
Thr70	Interior residue, hydrophobic interactions with Leu64, $O^{\gamma 1}$ with $C^{\delta 1}$ Asn67, C=O interaction with N-terminal α-NH_3^+	Thr70	Interior residue, hydrophobic interactions with Glu71, $C^{\gamma 1}$ with water, C=O interaction with N-terminal α-NH_3^+

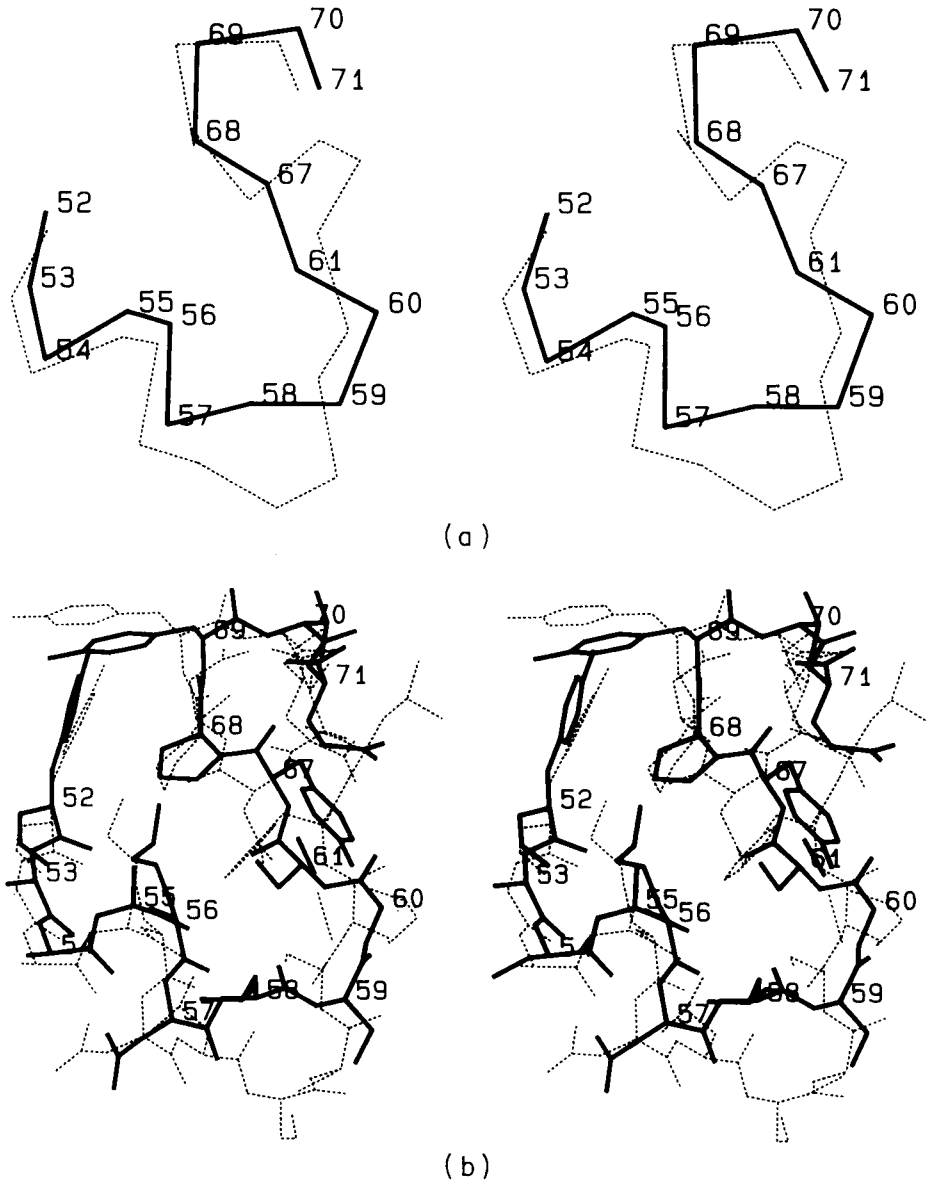

Figure 6. Comparison of the deletion region in wild-type porcine PLA_2 and the Δ62-66 mutant. The heavy lines represent the Δ62-66 mutant, the dotted lines represent the porcine PLA_2. (a) C^{α} atoms only; (b) all atoms.

closer (0·2 to 0·3 Å) to the disulfide bridge. The glycine at position 60 has ϕ, ψ values ($\phi = 67°$, $\psi = 43°$) close to the left-handed helix region. In 18 out of 21 snake venom phospholipases A_2 that have a deletion of five amino acid residues in this area there is a glycine residue at this position (Dennis, 1983). In the three exceptions it is Arg, Ser or Lys.

Tyr69 is located at the end of the loop. In the porcine PLA_2, Tyr69 is positioned at the entrance to the active center, pointing inwards to the active site of the protein. Since Pro68 has a different conformation, the C^{α} of Tyr69 is pulled towards the outside of the protein, and the side-chain is now pointing more towards the exterior of the protein. The difference in the O^{η} position is 5 Å. Leu2 moves to the position left by the tyrosine side-chain and fills up the newly created cavity (Fig. 8). As a result, the N-terminal helix gets a slightly different orientation. The N-terminal α-NH_3^+ moves 1·31 Å in one monomer and 1·10 Å in the other.

The active site itself, formed by residues His48, Asp99, Phe5, Ile9, Phe22, Ala102, Ala103, Phe106 and the disulfide bridge between Cys29 and Cys45 is hardly affected by the mutation (Dijkstra *et al.*, 1981, 1983). A superposition of these residues gives a r.m.s. difference of 0·43 Å between pairs of atoms between monomer 1 and the wild-type porcine enzyme and 0·40 Å for monomer 2 and the porcine PLA_2. The r.m.s. difference of these atoms between monomer 1 and monomer 2 is 0·33 Å.

One of the newly introduced residues is tyrosine 67. In many of the elapid snake venom PLA_2s there is an aromatic residue at this position (Dennis, 1983). This tyrosine residue is positioned at the

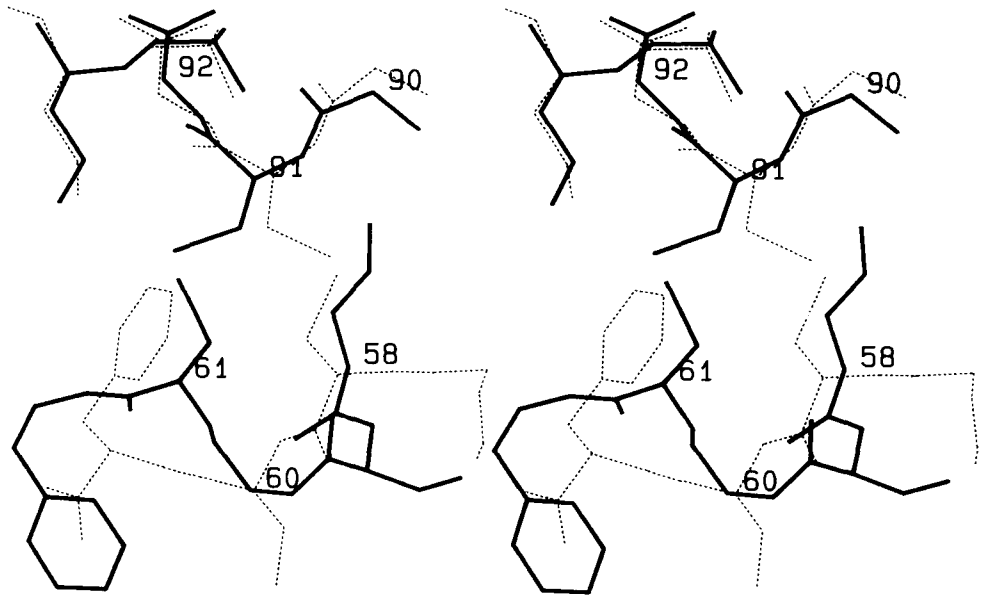

(a)

Fig. 7.

surface of the protein and it does not make any specific interactions. It might be a part of the binding site for aggregated substrates.

(d) *The second calcium-binding site*

The presence of a second calcium-binding site has been reported for porcine phospholipase A_2 based on both biochemical evidence and crystallographic work (Slotboom *et al.*, 1978; Andersson *et al.*, 1981; Donné-Op den Kelder *et al.*, 1983; Dijkstra *et al.*, 1983). This second calcium-binding pocket has a considerably lower affinity for calcium than the major site. From titration studies, it was found that Glu71 in the porcine PLA_2 is a ligand of this calcium ion (Donné-Op den Kelder *et al.*, 1983). In site-directed mutagenesis studies combined with activity measurements at high pH, Glu71 and Asp66 were identified as possible candidates for ligating the calcium ion. According to these studies, Glu92 would not be a ligand (van den Bergh *et al.*, 1989). In the crystal structure of wild-type porcine PLA_2, the calcium ion is bound on a crystallographic 2-fold axis and two symmetry-related molecules contribute to the binding of the calcium ion. As ligands, the carbonyl oxygen of Ser72, twice, and the $O^{\varepsilon 1}$ atom of Glu92, twice, were identified in the crystal structure. The two other ligands were thought to be water molecules but, due to the limited resolution of the porcine PLA_2 data, these water molecules were not visible in the electron density (Dijkstra *et al.*, 1983). Glu71 in the wild-type porcine PLA_2 structure is near the second calcium-binding site and through a simple rotation about the C^{γ}–C^{δ} bond, $O^{\varepsilon 1}$ or $O^{\varepsilon 2}$ could come into binding distance to the calcium ion. Residue 66 is too far away (≥ 10 Å) from the second calcium-binding pocket to be a direct ligand of the calcium ion (Dijkstra *et al.*, 1983).

In the crystal structure of the Δ62-66 mutant we also find this second calcium-binding site. This site is on the non-crystallographic 2-fold axis between two monomers. The calcium ion is surrounded by six ligands: the carbonyl oxygen of Ser72, twice, $O^{\varepsilon 1}$ of Glu92, twice, and $O^{\varepsilon 1}$ of Glu71, twice. The side-chain of Glu71 has rotated and it is now clearly a ligand of the calcium ion. The ligating residues make an optimum number of hydrogen bonds, both direct hydrogen bonds between residues from different monomers as well as hydrogen bonds mediated through water molecules (see Fig. 9). Thus, this calcium-binding site constitutes a region of strong interactions between the two monomers.

(e) *Comparison with* C. atrox *snake venom phospholipase* A_2

The only snake venom PLA_2 of which a detailed structure is available is the one from the Western diamondbacked rattle snake *Crotalus atrox* (Keith *et al.*, 1981; Brunie *et al.*, 1985). This *C. atrox* enzyme has a deletion of eight amino acid residues in the loop 56 to 70 compared with the pancreatic PLA_2s. On the basis of structural and sequential homology, it was concluded that residues 57, 58, 60 and residues 62 to 66 were deleted (Renetseder *et al.*, 1984).

Since a detailed comparison between the *C. atrox* PLA_2 and the bovine pancreatic PLA_2 has been given by Renetseder *et al.* (1984), we compare only the loop region from residues 52 to 70.

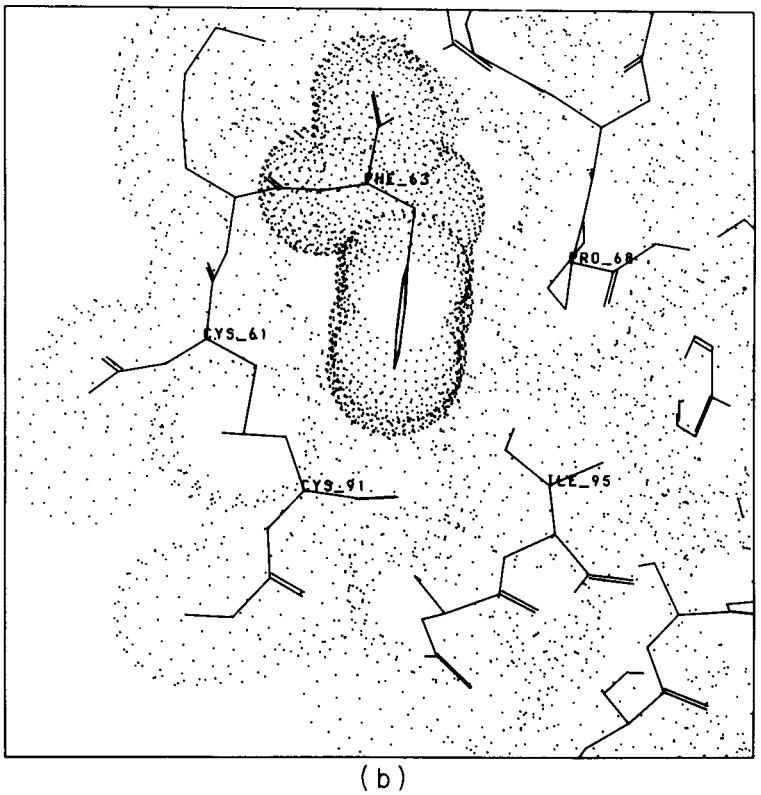

(b)

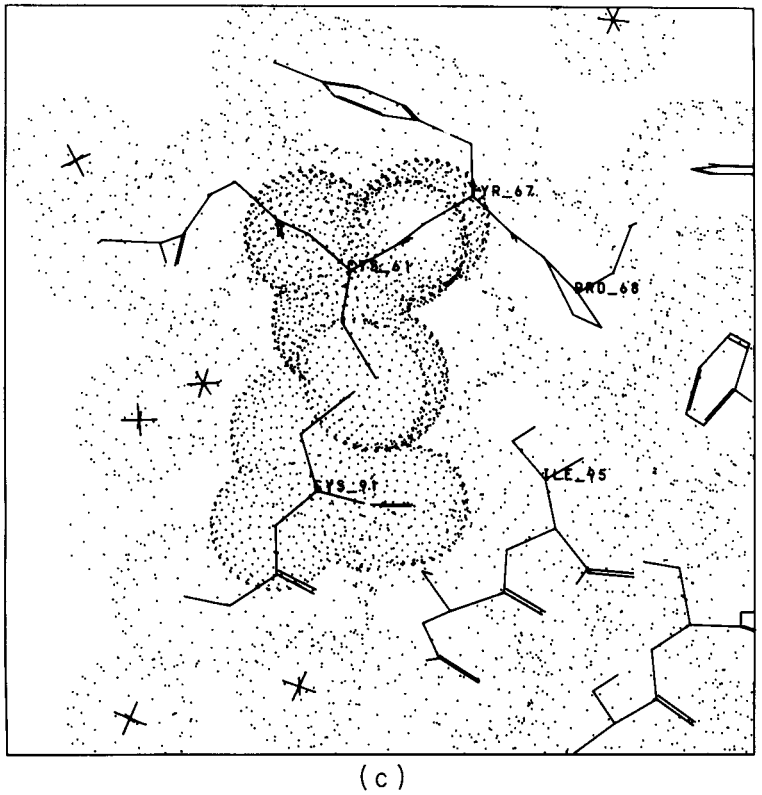

(c)

Figure 7. Comparison of the packing of the residues in the hydrophobic pocket in wild-type porcine PLA_2 and the Δ62-66 mutant. (a) Stereo drawing of the difference in conformation of the region around the disulfide bridge between residues 61 and 91. The heavy lines represent the Δ62-66 mutant, the dotted lines the porcine PLA_2. (b) The packing of residue 63 in the wild-type PLA_2. The heavy dots represent the van der Waals' surface of the atoms of Phe63. The other dots indicate the van der Waals' surface of the atoms of the rest of the protein. (c) The packing of the disulfide bridge 61–91 in the Δ62-66 mutant. The heavy dots represent the atoms of Cys61 and Cys91, the other dots indicate the van der Waals' surface of the other atoms of the Δ62-66 mutant structure.

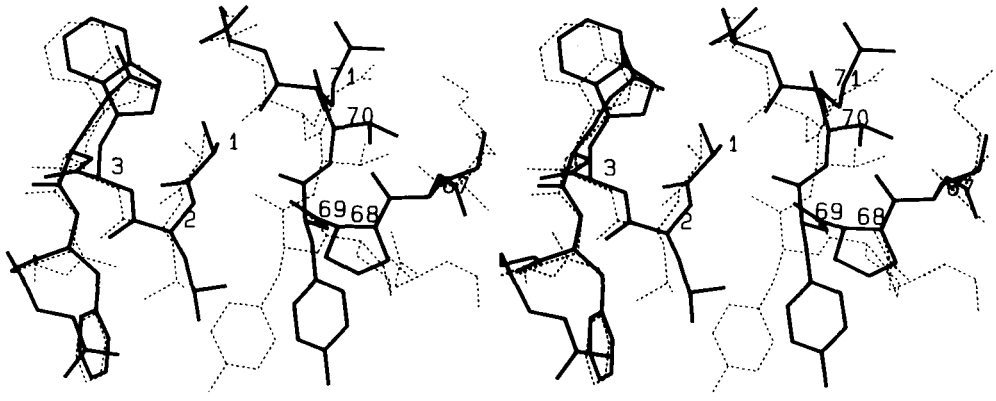

Figure 8. Comparison of the N-terminal loop and the loop from 67 to 70 in porcine PLA_2 (dotted lines) and in the Δ62-66 mutant (heavy lines), showing the concerted movement of Tyr69 and Leu2.

The main conformational difference between the Δ62-66 mutant and the *C. atrox* PLA_2 occurs before residue 61. The difference in structure of residues 61 to 70 is minimal. In order to allow the extra deletion of three residues, helix 40–58 is shortened by one and a half turns in the *C. atrox* enzyme. This helix terminates in the snake venom PLA_2 at position 52. Residues 53 to 55 have an extended conformation and residues 56 and 59 are located in a turn. In the mutant, the α-helix terminates at position 58 and the bend formed by residues 59 and 60 is located further on the outside of the protein (Fig. 10). Cys61 of the Δ62-66 PLA_2 mutant is located at almost the same position (the difference in C^{α} position is 1·1 Å).

4. Discussion

Above the structure of the Δ62-66 PLA_2 mutant and a comparison with the wild-type porcine PLA_2 and *C. atrox* snake venom PLA_2 are described. The biggest conformational differences occur around the deletion area, residues 62 to 66. The structure of this region in the mutant appears to be intermediate between that in wild-type porcine and *C. atrox* phospholipases A_2.

The enzyme has kept an internal hydrophobic area as conserved as possible by a relatively simple local adjustment of its conformation. While in the porcine wild-type PLA_2 Phe63 occupies a hydrophobic pocket, in the Δ62-66 mutant the disulfide bridge between Cys61 and Cys91 fills this hydrophobic pocket.

Due to a difference in crystallographic contacts the conformations around Leu31 in the two monomers are slightly different. In a comparison of the structures of bovine and porcine phospholipase A_2 (Dijkstra *et al.*, 1983) also a conformational difference in this region was found. Apparently this region has some conformational freedom. Also the regions around Pro14 and the C terminus appear to have some conformational freedom.

The Δ62-66 mutant has a second binding site for calcium similar to that found in the wild-type porcine PLA_2 structure. This site is on the non-crystallographic 2-fold axis relating the two monomers in the asymmetric unit. The side-chains of residues Glu71 and Glu92 and the carbonyl oxygen of residue 72 are ligands for this calcium ion. Although based on site-directed mutagenesis studies combined with activity measurements at high pH (van den Bergh *et al.*, 1989) Asp66 was suggested to be a ligand of the calcium ion instead of Glu92, this is extremely unlikely. In the crystal structure of wild-type porcine PLA_2 the Asp66 side-chain is more than 10 Å from the calcium ion, and in the present mutant structure, where Asp66 has been deleted, we still observe a second calcium ion bound at the same position as in the wild-type structure.

Kinetic studies with the Δ62-66 mutant show that this enzyme has a fully functional active site and a k_{cat}/K_m twice that of the wild-type porcine PLA_2 (Kuipers *et al.*, 1989*a*). The slight increase in activity towards monomeric substrates of this Δ62-66 mutant compared with wild-type porcine PLA_2 could be caused by small alterations in the active site. In the present 2·1 Å structure some changes around the active site can be detected, although the active site residues proper are, within error, identical between mutant and wild-type PLA_2. Due to the change in position of Tyr69, Leu2 moves to the newly created gap and the N-terminal α-helix changes slightly in orientation (1 to 1·3 Å at the N terminus). This observation of Leu2 coming towards Tyr69 has also been reported in filtered molecular dynamic runs on bovine PLA_2 by Sessions *et al.* (1989). In that paper, it was suggested that this movement changes the pocket between the two residues and that this might be important for adjusting the active site for the binding of monomeric substrates. Alternatively, the different position of Tyr69 could be responsible for the observed increase in activity. Tyr69 has been found to be important for the precise positioning of a phospholipid in the active site by binding to the phosphate group of the phospholipid (Kuipers *et al.*, 1989*b*). Another indication that there are indeed minute changes in the active site is the observation that this Δ62-66 mutant has a somewhat different binding constant for the calcium ion in the active

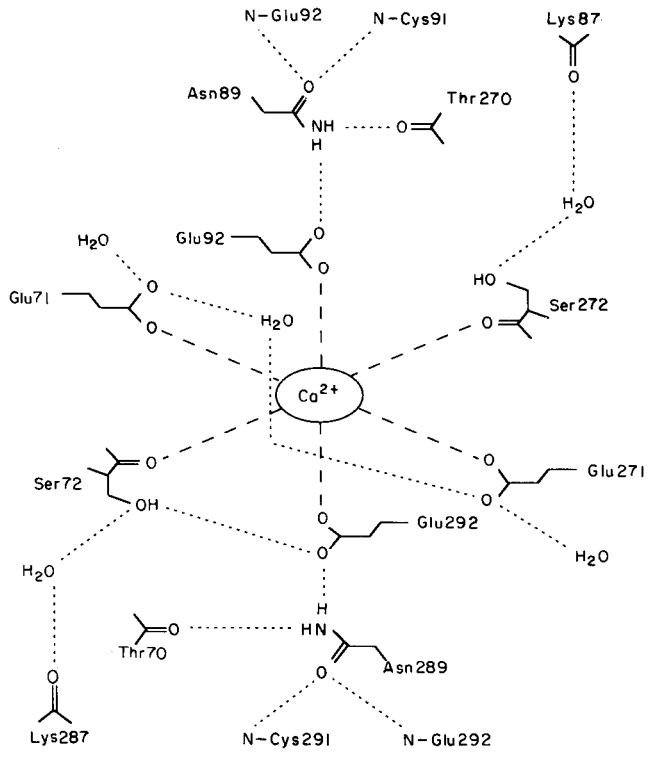

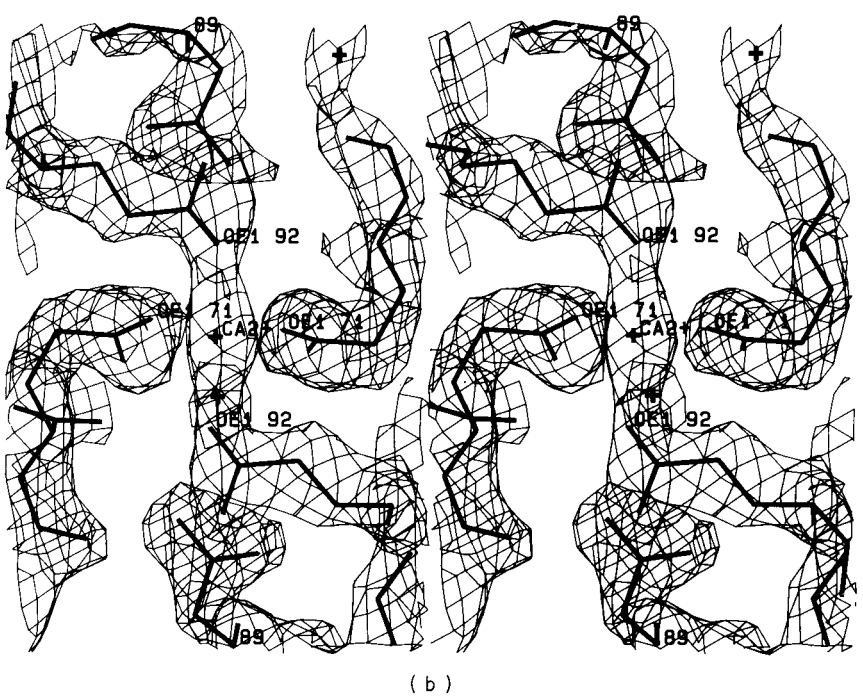

Figure 9. The surroundings of the 2nd calcium-binding site. (a) An overview of the ligands of the calcium ion and the hydrogen-bonding pattern surrounding this calcium-binding site. (b) $(2mF_o - DF_c)$, α_c map (Read, 1986) of the 2nd calcium-binding site. The density is contoured at $1{\cdot}1\sigma$.

center compared with wild-type porcine PLA_2. This binding constant changes from 1·8 mM to 0·8 mM at pH 6 in the Δ62-66 mutant (Kuipers *et al.*, 1989*a*).

The activity of the Δ62-66 mutant PLA_2 on aggregated short chain lecithins has increased up to 16-fold with respect to the wild-type enzyme (Kuipers *et al.*, 1989*a*). All residues identified to have interactions with the aggregated substrate molecules lie in a plane around the entrance to the active site on one face of the protein. Residues 64 to 66 in the wild-type porcine PLA_2 bulge out of the plane and form a protuberance. In the Δ62-66 PLA_2

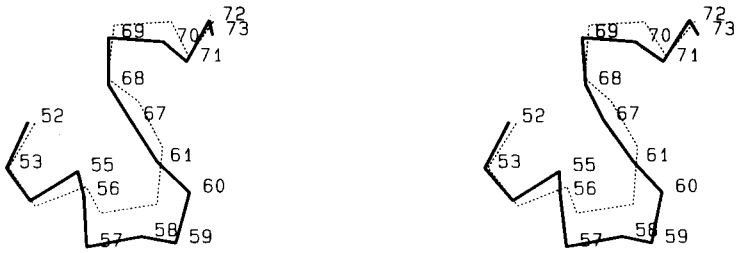

Figure 10. Comparison of C^{α} tracing of the deletion region in *C. atrox* PLA_2 (dotted lines) and the Δ62-66 mutant (heavy lines).

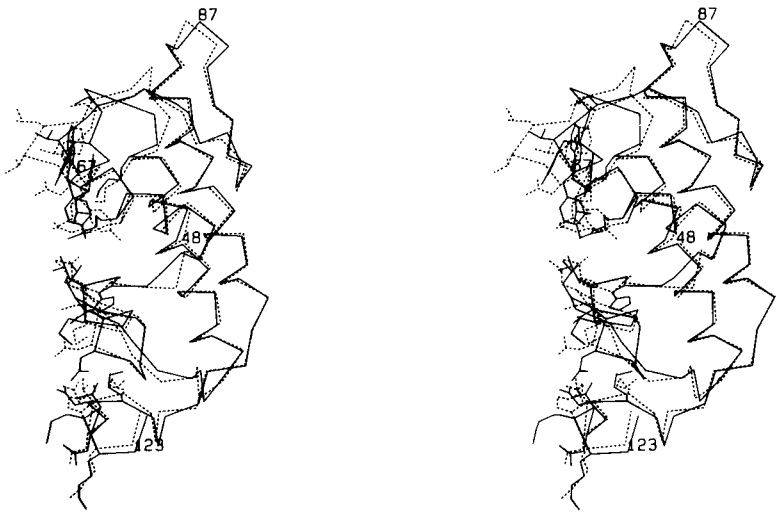

Figure 11. The putative binding site for aggregated substrates in wild-type (dotted lines) and Δ62-66 mutant PLA_2 (heavy lines). The side-chains are shown only for those residues presumed to be involved in the binding of phospholipid aggregates.

mutant these residues are deleted and the whole binding site forms now a smooth plane (Fig. 11). Although no structural details are known about the interaction of the enzyme with aggregated substrates, it is conceivable that due to this change in structure of the binding site for lipid aggregates, the enzyme's active site will have a somewhat different orientation towards the aggregated substrates. This might explain the difference in catalytic activity between the Δ62-66 mutant and the wild-type porcine PLA_2.

We thank Professor G. H. de Haas and his co-workers for their generous supply of protein material. The stimulating discussions with Professor W. G. J. Hol are gratefully acknowledged.

References

Andersson, T., Drakenberg, T., Forsén, S., Wieloch, T. & Lindström, M. (1981). Calcium Binding to Porcine Pancreatic Phospholipase A_2 Studied by ^{43}Ca NMR. *FEBS Letters*, **123**, 115–117.

Bhat, T. N. (1988). Calculations of an OMITMAP. *J. Appl. Crystallogr.* **21**, 279–281.

Bhat, T. N. & Cohen, G. H. (1984). OMITMAP: an Electron Density Map Suitable for the Examination of Errors in a Macromolecule. *J. Appl. Crystallogr.* **17**, 244–248.

Brünger, A. T. (1988). Crystallographic Refinement by Simulated Annealing: Application to a 2·8 Å Resolution Structure of Aspartate Amino Transferase. *J. Mol. Biol.* **203**, 803–816.

Brunie, S., Bolin, J., Gewirth, P. & Sigler, P. B. (1985). The Refined Structure of Dimeric Phospholipase A_2 at 2·5 Å. Access to a Shielded Catalytic Center. *J. Biol. Chem.* **260**, 9742–9747.

Dennis, E. A. (1983). Phospholipases. In *The Enzymes* (Boyer, P. D., ed.), 3rd edit., vol. 16, pp. 307–353, Academic Press, New York.

Dijkstra, B. W., Drenth, J. & Kalk, K. H. (1981). Active Site and Catalytic Mechanism of Phospholipase A_2. *Nature (London)*, **289**, 604–606.

Dijkstra, B. W., Van Nes, G. J. H., Kalk, K. H., Brandenburg, N. P., Hol, W. G. J. & Drenth, J. (1982). The Structure of Bovine Pancreatic Prophospholipase A_2 at 3·0 Å Resolution. *Acta Crystallogr. sect. B*, **38**, 793–799.

Dijkstra, B. W., Renetseder, R., Kalk, K. H., Hol, W. G. J. & Drenth, J. (1983). Structure of Porcine Pancreatic Phospholipase A_2 at 2·6 Å and Comparison with Bovine Phospholipase A_2. *J. Mol. Biol.* **168**, 163–179.

Dijkstra, B. W., Kalk, K. H., Drenth, J., de Haas, G. H., Egmond, M. R. & Slotboom, A. J. (1984). Role of the N-Terminus in the Interaction of Phospholipase A_2 with Aggregated Substrates. Properties and Crystal Structure of Transaminated Phospholipase A_2. *Biochemistry*, **23**, 2759–2766.

Donné-Op den Kelder, G. M., de Haas, G. H. & Egmond, M. R. (1983). Localisation of the Second Calcium Binding Site in Porcine and Equine Phospholipase A_2. *Biochemistry*, **22**, 2470–2478.

Fujinaga, M., Gros, P. & van Gunsteren, W. F. (1989). Testing the Method of Crystallographic Refinement using Molecular Dynamics. *J. Appl. Crystallogr.* **22**, 1–8.

Gros, P., Betzel, C., Dauter, Z., Wilson, K. S. & Hol, W. G. J. (1989*a*). Molecular Dynamics Refinement of a Thermitase-Eglin-C Complex at 1·98 Å Resolution and Comparison of Two Crystal Forms that Differ in Calcium Content. *J. Mol. Biol.* **210**, 347–367.

Gros, P., Fujinaga, M., Dijkstra, B. W., Kalk, K. H. & Hol, W. G. J. (1989*b*). Crystallographic Refinement by Incorporation of Molecular Dynamics: Thermostable Serine Protease Thermitase Complexed with Eglin-C. *Acta Crystallogr. sect. B*, **45**, 488–499.

Hall, S. R. & Stewart, J. M. (1987). Editors of *Xtal 2.2 User's Manual*, Universities of Western Australia and Maryland.

Hamilton, W. C., Rollet, J. S. & Sparks, R. A. (1965). On the Relative Scaling of X-ray Photographs. *Acta Crystallogr.* **18**, 129–130.

Jones, T. A. (1978). A Graphics Modelbuilding and Refinement System for Macromolecules. *J. Appl. Crystallogr.* **11**, 268–272.

Keith, C., Feldman, D. S., Deganello, S., Glick, J., Ward, K. B., Jones, G. D. & Sigler, P. B. (1981). The 2·5 Å Crystal Structure of a Dimeric Phospholipase A_2 from the Venom of *Crotalus atrox*. *J. Biol. Chem.* **256**, 8602–8607.

Kramer, R. M., Hession, C., Johansen, B., Hayes, G., McGray, P., Chow, E. P., Tizard, R. & Pepinsky, R. B. (1989). Structure and Properties of a Human Non-Pancreatic Phospholipase A_2. *J. Biol. Chem.* **264**, 5768–5775.

Kuipers, O. P., Thunnissen, M. M. G. M., de Geus, P., Dijkstra, B. W., Drenth, J., Verhey, H. M. & de Haas, G. H. (1989*a*). Enhanced Activity and Altered Specificity of Phospholipase A_2 by Deletion of a Surface Loop. *Science*, **244**, 82–85.

Kuipers, O. P., Dijkman, R., Pals, C. E. G. M., Verheij, H. M. & de Haas, G. H. (1989*b*). Evidence for the Involvement of Tyr69 in the Control of Stereospecificity of Porcine Pancreatic Phospholipase A_2. *Protein Eng.* **2**, 467–471.

Luzzati, V. (1952). Traitement Statistique des Erreurs dans la Determination des Structures Cristallines. *Acta Crystallogr.* **5**, 802–810.

Mizushima, H., Kudo, I., Horigome, K., Murakami, M., Hayakawa, M., Kim, D., Kondo, E., Tomita, M. & Inoue, K. (1989). Purification of Rabbit Platelet Secretory Phospholipase A_2 and its Characteristics. *J. Biochem.* **105**, 520–525.

Nieuwenhuizen, W., Dunze, H. & de Haas, G. H. (1974). Phospholipase A_2 (Phosphatide Acylhydrolase E.C.3.1.1.4.), from Porcine Pancreas. *Methods Enzymol.* **32b**, 147–154.

Pflugrath, J. W. & Messerschmidt, M. (1986). *Munich Area Detector NE System, User's Guide*, version 5.

Pieterson, W. A., Vidal, J. C., Volwerk, J. J. & de Haas, G. H. (1974). Zymogen Catalyzed Hydrolysis of Monomeric Substrates and the Presence of a Recognition Site for the Lipid-Water Interfaces on Phospholipase A_2. *Biochemistry*, **13**, 1439–1445.

Ramakrishnan, C. & Ramachandran, G. N. (1965). Stereochemical Criteria for Polypeptide and Protein Chain Conformations. II. Allowed Conformations for a Pair of Peptide Units. *Biophys. J.* **5**, 909–933.

Read, R. (1986). Improved Fourier Coefficients for Maps using Phases from Partial Structures with Errors. *Acta Crystallogr. sect. A*, **42**, 140–149.

Renetseder, R., Brunie, S., Dijkstra, B. W., Drenth, J. & Sigler, P. B. (1984). A Comparison of the Crystal Structures of Phospholipase A_2 from Bovine Pancreas and *Crotalus atrox* Venom. *J. Biol. Chem.* **260**, 11627–11634.

Seilhamer, J. J., Pruzanski, W., Vadas, P., Plant, S., Miller, J. A., Kloss, J. & Johnson, L. K. (1989). Cloning and Recombinant Expression of Phospholipase A_2 Present in Rheumatoid Arthritic Synovial Fluid. *J. Biol. Chem.* **264**, 5335–5338.

Sessions, R. B., Dauber-Osguthorpe, P. & Osguthorpe, D. J. (1989). Filtering Molecular Dynamics Trajectories to Reveal Low Frequency Collective Motions: Phospholipase A_2. *J. Mol. Biol.* **209**, 617–633.

Slotboom, A. J., Jansen, E. H. J. M., Vlijm, H., Pattus, F., Soares de Araujo, P. & de Haas, G. H. (1978). Calcium Binding to Porcine Pancreatic Phospholipase A_2 and its Function in Enzyme–Lipid Interaction. *Biochemistry*, **17**, 4593–4600.

Tronrud, D. E., ten Eyk, L. F. & Matthews, B. W. (1987). An Efficient General Purpose Least Squares Refinement Program for Macromolecular Structures. *Acta Crystallogr. sect. A*, **43**, 489–501.

van den Bergh, C. J., Bekkers, A., Verhey, H. M. & de Haas, G. H. (1989). Glutamic Acid 71 and Aspartic Acid 66 Control the Binding of the Second Calcium Ion in Porcine Phospholipase A_2. *Eur. J. Biochem.* **182**, 307–313.

van Eyk, J. H., Verhey, H. M., Dijkman, R. & de Haas, G. H. (1983). Interaction of Phospholipase A_2 from *Naja melanoleuca* Snake Venom with Monomeric Substrate Analogs. Activation of the Enzyme by Protein–Protein or Lipid–Protein Interactions? *Eur. J. Biochem.* **132**, 183–188.

Verhey, H. M., Egmond, M. R. & de Haas, G. H. (1981). Chemical Modification of the α-Aminogroup in Snake Venom Phospholipases A_2. A Comparison of the Interaction of Pancreatic and Venom Phospholipases with Lipid–Water Interfaces. *Biochemistry*, **20**, 94–99.

Volwerk, J. J. & de Haas, G. H. (1982). In *Lipid and Protein Interactions* (Jost, P. C. & Griffith, O. H., eds), vol. 1, pp. 69–149, Wiley, New York.

Vriend, G. (1990). WHATIF: A Molecular Modeling and Drug Design Program. *J. Mol. Graph.* **8**, 52–56.

Waite, M. (1987). *Handbook of Lipid Research*, vol. 5, Plenum, New York.

Edited by R. Huber